Accepted Manuscript

Using geologic structures to constrain constitutive laws not accessible in the laboratory

Johanna M. Nevitt, Jessica M. Warren, Kathryn M. Kumamoto, David D. Pollard

PII: S0191-8141(18)30038-5

DOI: 10.1016/j.jsg.2018.06.006

Reference: SG 3677

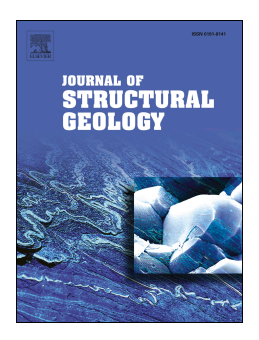
To appear in: Journal of Structural Geology

Received Date: 13 February 2018

Revised Date: 1 June 2018
Accepted Date: 3 June 2018

Please cite this article as: Nevitt, J.M., Warren, J.M., Kumamoto, K.M., Pollard, D.D., Using geologic structures to constrain constitutive laws not accessible in the laboratory, *Journal of Structural Geology* (2018), doi: 10.1016/j.jsg.2018.06.006.

This is a PDF file of an unedited manuscript that has been accepted for publication. As a service to our customers we are providing this early version of the manuscript. The manuscript will undergo copyediting, typesetting, and review of the resulting proof before it is published in its final form. Please note that during the production process errors may be discovered which could affect the content, and all legal disclaimers that apply to the journal pertain.



| 1 | Using geologic structures to constrain constitutive laws not accessible in the |
|----------|--|
| 2 | laboratory |
| 3 | Johanna M. Nevitt ^{a, *} , Jessica M. Warren ^b , Kathryn M. Kumamoto ^c , David D. Pollard ^c |
| 4 | |
| 5 | |
| 6 | ^a U.S. Geological Survey, 345 Middlefield Rd., MS-977, Menlo Park, CA 94025 |
| 7 | ^b Department of Geological Sciences, University of Delaware, Penny Hall, Newark, DE 19717 |
| 8 9 | ^c Geological Sciences Department, Stanford University, 450 Serra Mall, Building 320, Stanford CA 94305-2115, USA |
| 10 | |
| 11 | * Corresponding author: Tel.: +1 650 329 4855 (J.M. Nevitt). |
| 12 13 | <i>E-mail addresses:</i> jnevitt@usgs.gov (J.M. Nevitt); warrenj@udel.edu (J.M. Warren); kkumamot@stanford.edu (K.M. Kumamoto); dpollard@stanford.edu (D.D. Pollard) |
| 14 | |
| 15 | |
| 16 | |
| 17 18 | <i>Keywords:</i> constitutive laws, continuum mechanical modeling, equations of motion, rheology, microstructural analysis, brittle-ductile conditions, mantle shear zones |
| 19 | |
| 20 | |
| 21 | For submission to Journal of Structural Geology (40 th Anniversary Issue) |

Abstract

| In this essay, we explore a central problem of structural geology today, and in the foreseeable |
|---|
| future, which is the determination of constitutive laws governing rock deformation to produce |
| geologic structures. Although laboratory experiments provide much needed data and insights |
| about constitutive laws, these experiments cannot cover the range of conditions and |
| compositions relevant to the formation of geologic structures. We advocate that structural |
| geologists address this limitation by interpreting natural experiments, documented with field and |
| microstructural data, using continuum mechanical models that enable the deduction of |
| constitutive laws. To put this procedure into an historical context, we review the founding of |
| structural geology by James Hutton in the late 18 th century, and the seminal contributions to |
| continuum mechanics from Newton to Cauchy that provide the tools to model geologic |
| structures. The procedure is illustrated with two examples drawn from recent and on-going field |
| investigations of crustal and mantle lithologies. We conclude by pointing to future research |
| opportunities that will engage structural geologists in the pursuit of constitutive laws during the |
| 21 st century. |

1. Introduction

37

38

39

40

41

42

43

44

45

46

47

48 49

50

51

52

53

54

55

56

57

58 59

60

61

62

63

James Hutton (1726 – 1797) led a field trip along the east coast of Scotland in 1788. At Siccar Point he described what now is called Hutton's unconformity, where Devonian sandstone lies on the upturned edges of Silurian sandstone (Figure 1). Fragments of the Silurian beds are found in the basal conglomerate just above the unconformity. John Playfair (1748 – 1819), Professor of Natural Philosophy at the University of Edinburgh, accompanied Hutton to Siccar Point and provided the following commentary (McIntyre and McKirdy, 2012, p. 45): "On us who saw these phenomena for the first time, the impression made will not easily be forgotten. The palpable evidence presented to us [by Hutton] of one of the most extraordinary and important facts in the natural history of the earth, gave a reality and substance to those theoretical speculations, which, however probable, had never till now been directly authenticated by the testimony of the senses. We often said to ourselves, what clearer evidence could we have had of the different formation of these rocks, and of the long interval which separated their formation, had we actually seen them emerging from the bosom of the deep? We felt ourselves necessarily carried back to the time when the [Silurian] schistus on which we stood was yet at the bottom of the sea, and when the [Devonian] sandstone before us was only beginning to be deposited, in the shape of sand or mud, from the waters of a super-incumbent ocean. An epoch still more remote presented itself, when even the most ancient of these rocks, instead of standing upright in vertical beds, lay in horizontal planes at the bottom of the sea, and was not yet disturbed by the immeasurable force which has burst asunder the solid pavement of the globe." Church dogma, well known to Hutton and Playfair, reckoned the age of Earth to be 6,000 years, and recorded the only natural event that might disturb the "solid pavement of the globe" as the biblical story of Noah's flood. Challenging that dogma, Hutton used the geometry of the juxtaposed sedimentary formations and kinematic reasoning to deduce

| 64 | their relative ages, and he used his principle of uniformitarianism to argue for much |
|----|---|
| 65 | longer time and much greater force. With these insights, and many others, Hutton |
| 66 | founded the scientific discipline of geology (McIntyre and McKirdy, 2012), and laid the |
| 67 | cornerstones for the sub-discipline of structural geology. |
| 68 | The "long interval" separating the formation of the juxtaposed sedimentary formations at |
| 69 | Siccar Point (Figure 1) has been quantified by sedimentologists, paleontologists, and |
| 70 | geochronologists over the ensuing two centuries (e.g. Brown et al., 2002). The upright Silurian |
| 71 | sandstones were deposited about 435 Ma, and the Devonian conglomerate and sandstones were |
| 72 | deposited about 370 Ma, so Hutton's unconformity represents about 65 million years of |
| 73 | unrecorded geologic history. Today, the "immeasurable force" is routinely recorded using in-situ |
| 74 | stress measurement techniques (Amadei and Stephansson, 1997), and models constructed using |
| 75 | continuum mechanics (Ramsay and Lisle, 2000; Pollard and Fletcher, 2005; Turcotte and |
| 76 | Schubert, 2014) quantitatively account for the motions and forces involved in the formation of |
| 77 | structures like those described by Hutton. |
| 78 | Because Sir Isaac Newton (1642 – 1726) published <i>The Principia</i> in 1687 (Newton, |
| 79 | 1999), 100 years before the field trip to Siccar Point, one might wonder why Hutton and his |
| 80 | colleagues did not relate the forces they imagined to the motions and relative motions they |
| 81 | deduced from outcrop observations? We presume they knew that Newton's Second Law of |
| 82 | Mechanics provided the relationship, $\mathbf{F} = m\mathbf{a}$, between the force vector, \mathbf{F} , applied to a particle of |
| 83 | mass m , and the resulting acceleration vector, \mathbf{a} . However, the rocks at Siccar Point were |
| 84 | composed of a vast collection of particles, forming a continuous body in which every particle |
| 85 | was acted upon by its neighbors, and the entire collection of particles deformed due to some |

remotely applied forces. Thus, while Newton's relationship may have seemed relevant to those on the 1788 field trip, it would not have been obvious how to apply it.

The insights necessary to apply Newtonian mechanics to that vast collection of particles were being developed at about the same time (Malvern, 1969; Lai et al., 2009). In the middle of the 18th century the spatial description of motion was introduced that provides the kinematic framework for fluid dynamics, and now is associated with the work of Leonhard Euler (1707 – 1783). About that same time, the referential description of motion was introduced that provides the kinematic framework for solid dynamics, and now is associated with the work of Joseph-Louis Lagrange (1736 – 1813). In 1827, shortly after Hutton's death, Augustine-Louis Cauchy (1789 – 1857) introduced the general equations of motion for a continuous body and the stress tensor, which accounts for the mechanical actions of particles on their neighbors. Cauchy's First and Second Laws of Motion are (e.g Pollard and Fletcher, 2005, Section 7.3):

98
$$\bullet \frac{Dv_i}{Dt} = \frac{\bullet \bullet_{ji}}{\bullet x_j} + \bullet g_i, \quad i, j = 1, 2, 3$$

$$\bullet_{ij} = \bullet_{ji}, \quad i \bullet j$$
(1)

where the operator D/Dt is the material time derivative. In these equations the dependent variables are the velocity vector components, v_i , and the stress tensor components, \bullet_{ij} ; the independent variables are the spatial coordinates, x_i , and time, t. The only material property is mass density, \bullet , and components of the gravitational acceleration vector are g_i . The left side of the first equation accounts for mass times acceleration, and the right side accounts for the resultant forces, so this is the embodiment of Newton's Second Law for the continuum.

<u>ØCEPTED MANUSCRIPT</u>

| Cauchy's Laws of Motion apply to all rock types under all possible conditions of |
|--|
| temperature, pressure, and rate of deformation in Earth's lithosphere and asthenosphere. They |
| apply to rock that is brittle, ductile, or fluid, and to geologic structures of all types, including |
| fractures, faults, folds, fabrics, and intrusions. If used alone, they describe the mechanical |
| behavior of a rock mass that is isothermal and isochemical. In this brief essay, we focus on the |
| mechanical aspects of rock deformation, because they often dominate the other physical and |
| chemical processes operating during the formation of geologic structures, but we acknowledge |
| that heat and mass transport, and chemical reactions can be important parts of a comprehensive |
| analysis (Hobbs and Ord, 2014). |

By the second half of the 19th century, what we now call continuum mechanics was firmly established in the standard tool set of physicists and engineers to address the deformation of elastic bodies and the flow of viscous fluids. While foundational in their generality, Cauchy's Laws of Motion are impractical to apply directly, because they contain too many dependent variables (3 velocity components and 6 stress components). The key to applying these equations is the introduction of constitutive laws, which define the relationship between stress and strain or the rate of deformation. Constitutive laws not only introduce mechanical properties that can be quantified for rock, they also reduce the number of dependent variables to equal the number of equations. For example, by relating stress to the rate of deformation for a linear viscous fluid, the stress components are eliminated from Cauchy's Laws, which then become the three Navier-Stokes equations for fluid dynamics, with only three dependent velocity components (e.g. Pollard and Fletcher, 2005, Section 7.4).

Throughout the 20th century, a building cohort of structural geologists exploited linear elastic and linear viscous theory to investigate the deformation of rock during the formation of

| 128 | geologic structures (Johnson, 1970; Hubbert, 1972; Ramsay and Lisle, 2000). In parallel with |
|-----|--|
| 129 | those investigations, laboratory studies of the mechanical properties of rock confirmed the |
| 130 | efficacy of the linear constitutive laws, but recognized and quantified significant non-linear |
| 131 | aspects of rock deformation (e.g., Griggs, 1939; Paterson, 1958; Kohlstedt and Goetze, 1974). |
| 132 | Rock mechanics laboratory studies typically are carried out on cylindrical rock samples, |
| 133 | rarely greater than a decimeter in length. They represent particular lithologies with a grain size |
| 134 | that usually is very small compared to the sample dimensions, so the samples are homogeneous |
| 135 | at the sample scale (Tullis and Tullis, 1986; Paterson and Wong, 2005; Jaeger et al., 2009). |
| 136 | Loading usually is axisymmetric with an axial stress that is the greatest compression and a radial |
| 137 | stress (confining pressure) that is the least compression. Pore fluid pressure less than the |
| 138 | confining pressure may be applied to jacketed samples. Some data is available from true triaxial |
| 139 | tests on cubic samples, but the cylindrical sample with axisymmetric loading is the standard. |
| 140 | Servo-controlled systems prescribe changes in loading, displacement, or displacement rate, as |
| 141 | well as temperature, confining and pore pressure. To obtain results on a human timescale, most |
| 142 | experiments are conducted at a strain rate greater than 10^{-7} s ⁻¹ , which requires ~12 days to |
| 143 | produce 10% strain in the sample. Shear zones in the lower crust and upper mantle, however, |
| 144 | likely develop under strain rates of 10^{-12} to 10^{-15} s ⁻¹ (e.g., Boettcher et al., 2007). To account for |
| 145 | this discrepancy, experimentalists strategically offset fast strain rates with high temperatures, and |
| 146 | flow laws constrained in the laboratory must be extrapolated across several orders of magnitude |
| 147 | before ultimately applying them to geologic structures (e.g., Paterson, 1987). While some of the |
| 148 | limited ranges of laboratory conditions will be expanded in the future, nature is not so |
| 149 | constrained. |

Structural geologists address many limitations of laboratory tests by interpreting natural experiments, documented with field data, using mechanical models that enable the deduction of governing constitutive laws and properties (e.g., Bürgmann and Pollard, 1994; Treagus, 1999; Kenis et al., 2005; Hudleston and Treagus, 2010; Mancktelow and Pennacchioni, 2010; Grigull et al., 2012). Microstructural analysis provides an additional tool for evaluating laboratory-derived constitutive laws extrapolated to geologic conditions (e.g., Hirth et al., 2001; Cross et al., 2015). In this paper, we illustrate the procedure with two examples drawn from recently published (Section 2) and on-going (Section 3) field investigations of structures exhumed from the mid-crust and upper mantle, respectively. We conclude by pointing to future research opportunities that will engage structural geologists in the pursuit of constitutive laws during the 21st century.

2. Probing constitutive laws for faulting under brittle-ductile

conditions

The brittle-ductile transition is an interval of Earth's lithosphere where deformation occurs by a combination of brittle (e.g., fracturing), crystal plastic (e.g., dislocation creep), and/or solution mass transfer mechanisms (e.g., Kirby, 1983; Scholz, 1988). In quartzofeldspathic continental crust, this zone occurs between depths corresponding to ~300°C and ~450°C, where quartz deforms plastically around brittle feldspar porphyroclasts (e.g., Tullis, 2002; Passchier and Trouw, 2006). The brittle-ductile transition has long intrigued geoscientists, because it hosts peak lithospheric strength (Brace and Kohlstedt, 1980; Kohlstedt et al., 1995) and the foci for many large-magnitude earthquake ruptures (Sibson, 1982, 1983). Despite the academic interest and direct relevance to seismic hazard analysis, significant uncertainty still

surrounds fault mechanics in this region, due largely to the lack of constraints on appropriate constitutive laws for mixed brittle and plastic mechanisms.

Ancient, exhumed faults offer windows into fault behavior under brittle-ductile conditions. Over the last four decades, the Mount Abbot Quadrangle of the central Sierra Nevada, California, has served as a key field site for such investigations. Here we focus on meter-scale strike-slip faults in the Lake Edison granodiorite, located in the south-central part of the quadrangle (Lockwood and Lydon, 1975). Offset dikes and xenoliths indicate left-lateral slip for the majority of faults, which developed due to reactivation of pre-existing joints (Segall and Pollard, 1983). Left and right steps commonly separate fault segments, producing regions of enhanced extension and contraction, respectively (Segall and Pollard, 1980). In many cases, extensional steps contain opening-mode fractures, while granodiorite within contractional steps is strongly mylonitized (Bürgmann and Pollard, 1992, 1994). Microstructural analysis and geobarometric data indicate deformation occurred at ~300-500°C under a confining pressure of ~250 MPa, consistent with the brittle-ductile transition (Griffith et al., 2008; Pennacchioni and Zucchi, 2013; Nevitt et al., 2017a).

We targeted the Seven Gables outcrop (Figure 2) to serve as the foundation for a mechanical model (Nevitt et al., 2014; Nevitt et al., 2017b). The outcrop contains a contractional right step between two left-lateral fault segments offsetting a once-continuous leucocratic dike. Stretch and rotation of the dike record finite deformation within the step, providing a valuable benchmark for comparison with model results. In addition, a locally strong mylonitic fabric developed in the dike and adjacent granodiorite within the step. We quantitatively determined the fabric distribution by calculating the axial ratio and orientation of each visible mafic grain (Figure 2B; Nevitt et al., 2017b). We consider grains with axial ratios 3 and trends consistent

with the deformed dike and faults to represent the step-related fabric. This fabric is strongest in the center of the step between the fault tips and decays outward, forming a sigmoidal pattern.

Microstructural analysis provides valuable insight into deformation mechanisms and relevant constitutive laws. We analyzed samples of the dike and granodiorite collected outside and inside the step, representative of the regional fabric and step-related fabric, respectively (Nevitt et al., 2017b). An S-C mylonitic foliation (Lister and Snoke, 1984) developed both in the granodiorite and dike within the step where the S-plane is defined primarily by a shape-preferred orientation in recrystallized quartz. The C-plane is defined by aligned biotite grains in the granodiorite and fine-grained feldspar grains in the dike. In both lithologies, the presence of subgrains, interlobate grain boundaries, and a strong crystallographic preferred orientation indicate quartz deformed by dislocation creep. Feldspar grains commonly contain microfractures, but also exhibit bent twinning, flame perthite, and irregular grain boundaries, suggesting semi-brittle deformation. In the granodiorite, biotite grew stably in pressure shadows of feldspar porphyroclasts, indicative of pressure solution, and rarely kinked or fractured. Hornblende and sphene deformed by brittle fracturing. Thus, deformation involved a complex combination of mechanisms down to the grain-scale, further confounding the choice of constitutive law.

We developed a conceptual understanding of the step deformation through kinematic models based on geometric constraints (Nevitt et al., 2014). Initially, the approximately planar dike dipped 25° to the NE and was cross-cut by two right-stepping joints with 10 cm of overlap. As the joints were reactivated as left-lateral faults, the dike segment within the step rotated counterclockwise about a non-vertical axis, resulting in a 61° dip to the NNE. The fault tips deflected outward from the step, accounting for extension in the direction orthogonal to the fault

trends. Taking into account rotation about a non-vertical axis, the dike apparently maintained constant volume during deformation.

217

218

219

220

221

222

223

224

225

226

227

228

229

230

231

232

233

234

235

236

237

238

239

This kinematic understanding provides the context for a mechanics-based finite element model of the deformation (Nevitt et al., 2017b). Finite element analysis is a numerical method of solving boundary value problems for partial differential equations, including the equations of motion, in a continuum (Hughes, 2000). We used Abaqus/Standard (https://www.3ds.com/products-services/simulia/products/abagus/), a commercial quasi-static solver, to construct and evaluate models that test the ability of various constitutive equations to reproduce deformation documented in the Seven Gables outcrop. The starting fault and dike geometries in the 2D plane strain model come directly from field measurements and the kinematic reconstruction. The left and bottom boundaries are fixed in the x- and y-directions, respectively, while loading is introduced in two steps (Figure 3A): (1) Isotropic lithostatic pressure of 250 MPa; (2) Bulk contraction oblique to the faults to initiate left-lateral fault slip. The orientation of bulk contraction relative to the faults is based on that of splay fractures observed in the field, interpreted to indicate the orientation of the most compressive principle stress. Fault slip is governed by the Coulomb criterion (Coulomb, 1773), in which the driving shear stress must exceed a critical value related to the fault's frictional strength and normal stress.

With the same starting geometry, boundary conditions, and loading procedure, we ran the model five times with different candidate constitutive laws for describing brittle-ductile deformation: (1) Von Mises elastoplasticity, (2) Drucker-Prager elastoplasticity, (3) Viscoelastic power law creep, (4) Coupled elastoviscoplasticity, and (5) Two-layer elastoviscoplasticity (Nevitt et al., 2017b). Here, we focus on results from the first three models, which cover the

each fault tip.

| range of representative results. Both elastoplasticity and viscoelasticity may produce permanent, |
|---|
| non-recoverable deformation. An important distinction between these two types of constitutive |
| laws is that elastoplasticity requires the stress state to meet a criterion for plastic yielding, while |
| viscous creep can occur under any stress state given enough time. The Von Mises (Von Mises, |
| 1913) and Drucker-Prager (Drucker and Prager, 1952) yield criteria are commonly used to |
| characterize elastoplastic deformation in metals and geologic materials, respectively. While the |
| Von Mises criterion is independent of mean normal stress (i.e., pressure), yield strength in the |
| Drucker-Prager criterion increases with increasing mean normal stress. |
| Models implementing these elastoplastic and viscoelastic constitutive laws produce |
| distinct strain distributions (Figure 3C-E). Notably, the Von Mises model (Figure 3C) strictly |
| localizes shearing along the faults and within the step, while the Drucker-Prager model (Figure |
| 3D) concentrates strain outside the step, and the viscoelastic model (Figure 3E) distributes |
| deformation more broadly across the model domain. The Von Mises model provides the closest |
| match to the outcrop deformation. Compared with outcrop measurements of dike rotation (44°), |
| stretch (3.3), and offset (30 cm), the model dike reaches values of 48°, 3.2, and 26 cm, |
| respectively. In addition, the model strain distribution mimics that observed in outcrop (Figure |
| 2B), with strain sharply confined within the faults and the greatest magnitudes occurring |
| diagonally through the center of the fault step. Contrary to field observations, strain in the |
| Drucker-Prager elastoplastic model focuses near the fault tips outside the step and the fault tips |
| deflect inward toward the step's center. The viscoelastic power law creep model, which required |
| a high strain rate of 10 ⁻⁴ s ⁻¹ to prevent stress relaxation and stimulate fault slip, produces strain |
| both within and outside the step with the greatest values occurring nearly symmetrically about |
| |

With these new constraints, we further investigated fault behavior under brittle-ductile conditions by constructing finite element models with multiple fault steps and Von Mises elastoplastic behavior (Nevitt and Pollard, 2017). In agreement with mapped fault systems in the Mount Abbot Quadrangle, we found that modeled off-fault plastic yielding enhanced fault tip interaction and slip transfer. This allows faults to attain greater slip magnitudes and gradients than for modeled faults in a linear elastic medium or for natural faults active at Earth's surface (e.g., Dawers et al., 1993), where a frictional rheology given by Byerlee's law is expected. Thus, the combined methodology of geologic observations and continuum mechanics illuminates new and significant characteristics of fault behavior at the base of the seismogenic zone.

3. Constraints on multiphase constitutive laws for upper mantle

deformation

Plate boundary deformation below the brittle-ductile transition is dominated by bulk plastic flow that facilitates shear localization (e.g., Scholz, 1988). Such deformation is essential to plate tectonics, since the relative motions of rigid lithospheric plates require localized deformation at their boundaries. Because most lithospheric material consists of the upper mantle, constraining flow laws (i.e., constitutive laws defining viscous flow) for peridotite and its constituent minerals, olivine and pyroxene, is crucial to understanding the mechanics driving plate motions and the strength of the lithospheric mantle.

While laboratory experiments have significantly advanced knowledge of olivine constitutive behavior (e.g., Hirth and Kohlstedt, 2003), flow laws for other mantle materials remain poorly constrained. Experiments on orthopyroxene face the challenges of obtaining suitable starting material and working at restricted pressure-temperature conditions to prevent low-pressure polymorphs (e.g., Raleigh et al., 1971; Skemer and Karato, 2007; Bystricky et al., 2016). For polyphase materials (e.g., peridotite), laboratory conditions are similarly limited due to chemical interaction and partial melting (Ji and Xia, 2002). Even for olivine, while strains up to ~20 have been achieved in experiments (e.g., Hansen et al., 2014), naturally deformed samples can reach much greater magnitudes (Figure 4). Hence, field studies of naturally deformed peridotite are necessary to test the appropriateness of laboratory-derived flow laws under mantle conditions over geologic timescales.

The Josephine Peridotite in the western Klamath Mountains, Oregon, is a prime field site for studying constitutive laws governing mantle deformation, along with mechanisms leading to

| shear localization. The Fresno Bench section of this obducted peridotite massif is a 1 km wide | |
|---|--|
| glacial step that contains >10 well-exposed, small-scale shear zones (Figure 4, Supporting | |
| Material). The shear zones share broadly similar compositions, consisting mainly of harzburgite | |
| (~70% olivine, 30% orthopyroxene) with some interlayered dunite (100% olivine). Melt is | |
| evident in the center of some shear zones, either as gabbro veins, pyroxenite veins, or dunite. | |
| Strain can be measured due to the presence of a pyroxene foliation that has relief on outcrops due | |
| to preferential weathering of olivine relative to pyroxene (Figure 4A). As the presence of a strain | |
| marker in peridotite is unusual, this locality provides unique constraints on deformation of | |
| olivine and pyroxene under natural conditions (e.g., Loney and Himmelberg, 1976; Kelemen and | |
| Dick, 1995; Warren et al., 2008). | |
| | |

Mapped deflections of the pyroxene foliation (Figure 4B) combined with kinematic techniques traditional to structural geology (e.g., Ramsay, 1980) have been used to calculate strain profiles across each shear zone (Figure 4C). Shear zone width ranges from 2.5 m to 60 m and maximum strain ranges from 1.6 to > 64 (Supporting Material). Interestingly, some shear zones are characterized by asymmetric strain profiles, possibly indicating interaction between neighboring structures. Deformation features observed in these shear zones may provide important insight into the micromechanics and governing constitutive laws for shear localization. For example, Skemer et al. (2013) compared measurements from Shear Zone P to results of a 1D numerical model that incorporated an empirical flow law, an analytical solution to the diffusion equation, and an empirical function for viscous anisotropy. By varying water content and viscous anisotropy in the model, they determined that strain localization required at least two micromechanical processes (i.e., water weakening and the development of lattice preferred orientation).

| Microstructural and compositional variations among the shear zones provide additional |
|--|
| insight into the role of grain size, melt, water content, secondary phase abundance, and mineral |
| alignment (i.e., viscous anisotropy) on constitutive behavior (Warren et al., 2008; Skemer et al., |
| 2010; Recanati et al., 2012; Skemer et al., 2013; Hansen and Warren, 2015). Here we use data |
| from these shear zones to evaluate the application of laboratory-derived constitutive laws for |
| olivine aggregates (i.e., dunite) to multiphase aggregates (i.e., harzburgite). The misfit between |
| predictions from laboratory-derived laws and observations of natural samples suggests that |
| continuum mechanics modeling may improve constraints on constitutive behavior and could be |
| used to expand the 1D analysis of shear localization by Skemer et al. (2013) to higher |
| dimensions. |

Outcrop observations and microstructural analyses of harzburgite and dunite indicate that olivine deformation occurred by dislocation-accommodated grain boundary sliding (disGBS) (Hansen and Warren, 2015). Laboratory experiments (Bystricky et al., 2016) and field observations (Tikoff et al., 2010) indicate greater viscosity for pyroxene compared to olivine. However, interlayered harzburgite and dunite are co-deformed in one of the Josephine shear zones with no macroscopic evidence (e.g., boudinage or folding) for a viscosity difference between the two lithologies. Hansen and Warren (2015) observed that olivine grain size decreases with increasing pyroxene fraction in the shear zone, following a Zener pinning relationship (Linckens et al., 2014). Thus, they concluded that olivine deformed by a grain-size sensitive mechanism, in which viscosity decreases with decreasing grain size. This would account for the approximately uniform viscosity of the dunite and harzburgite with the decreased olivine viscosity due to grain size reduction in the harzburgite offsetting the higher viscosity expected from the presence of pyroxene. Olivine microstructural data for the Josephine shear

zones plot within the laboratory-determined disGBS field, but only when assuming anhydrous conditions (Figure 5A; Hansen and Warren, 2015).

350

351

352

353

354

355

356

357

358

359

360

361

362

363

364

365

366

367

368

369

370

371

372

Our estimates of olivine water content, however, suggest relatively hydrous conditions during deformation, with olivine containing 200–600 ppm H/Si (equivalent to 13–38 ppm H₂O) across the Fresno Bench outcrop (Kumamoto, 2018). Using hydrous olivine flow laws at the estimated depth (~30 km) and temperature (~1000°C) conditions of Josephine Peridotite deformation, the differential stress required for wet disGBS is unreasonably high (>1 GPa; Ohuchi et al., 2015). Instead, the Josephine data plot across the intersection of the wet diffusion and dislocation creep fields (Figure 5B), with deformation accommodated by 10-60% diffusion creep and 40-90% dislocation creep. This combination of mechanisms allows for some deformation to be accommodated by a grain-size sensitive mechanism (i.e., diffusion creep), which matches the outcrop and microstructural observations, while accommodation by dislocation creep can account for the occurrence of an olivine lattice preferred orientation. However, as the contribution of diffusion creep increases, the olivine fabric strength should decrease (e.g., Warren and Hirth, 2006). In contrast, Hansen and Warren (2015) observed a constant fabric strength with varying grain size and modal pyroxene. Hence, the Josephine Peridotite microstructural data further suggest that deformation was accommodated by wet disGBS, despite the mismatch with existing laboratory data for this mechanism.

The discrepancy between microstructural observations of deformed peridotites and the empirical disGBS flow law indicates that additional factors are needed in the extrapolation to natural conditions. The wet disGBS flow law is calibrated by a limited number of high pressure (1.5-6.7 GPa) experiments on olivine aggregates (Ohuchi et al., 2015), but refinement of the parameters is unlikely to expand the field to the lower stresses in Figure 5B. Experiments

| conducted at lower pressure (300 MPa) have found no evidence for disGBS in hydrous olivine |
|---|
| (Tasaka et al., 2016). Instead, we suggest that the discrepancy may be related to the polyphase |
| nature of natural peridotite. Hirth and Kohlstedt (2003) suggested that wet disGBS does not |
| occur because dislocation climb is enhanced by the presence of water. However, the presence of |
| pyroxene may require increased activation of grain boundary sliding to accommodate |
| deformation, if the occurrence of mixed phase boundaries (e.g., olivine-orthopyroxene) offsets |
| the enhanced mobility of dislocations when water is present. Thus, wet disGBS may be active |
| over an expanded range of conditions for olivine-pyroxene aggregates than for pure olivine. |

Quantification of constitutive behavior in this system is necessary to constrain strength. The Josephine data correspond to a strain rate approximately one order of magnitude faster assuming hydrous rather than anhydrous deformation conditions (Figure 5). Further weakening would be expected for hydrous polyphase disGBS relative to hydrous dislocation creep, which would enhance shear localization. Fundamentally, extrapolating flow laws from laboratory to natural conditions relies on the assumption that the same microphysical processes control rheological behavior in both settings (e.g., Hirth and Kohlstedt, 2003), and microstructural analysis provides a tool to test this assumption (e.g., Wallis et al., 2017).

We suggest that continuum mechanics provides an additional tool to search for multiphase flow laws that reproduce field observations. Similar to the example in Section 2, a numerical experiment could be designed in which the model geometry and boundary conditions are derived directly from detailed field maps of the Josephine shear zones. Application of novel techniques, such as photogrammetry (e.g., Bemis et al., 2014), may allow three-dimensional structures to be extracted from this outcrop to provide a similar level of constraints as is currently available for the Seven Gables outcrop. By prescribing a remote displacement boundary

condition consistent with field measurements and applying representative pressure-temperature conditions, the constitutive law and input parameters could be varied to compare the resulting deformation with that recorded by the strain profiles. These models could be evaluated against future experimental data, as new types of experiments (e.g., Cyprych et al., 2016; Cross & Skemer, 2017; Zhao et al., 2017) lead to improved constraints on the extrapolation of single-phase flow laws to the multiphase domain. Additionally, this methodology could reveal how ductile shear zones interact with each other, potentially accounting for the observed asymmetric strain profiles in Figure 4C. Ultimately, this type of modeling is important for understanding how plate boundaries form in the mantle, for example at oceanic transform faults.

4. Discussion: Future research opportunities

The methodology outlined above – combining field and microstructural measurements with mechanical models to deduce constitutive laws – is likely to provide important insights into outstanding questions in structural geology and tectonics. The open questions of how rheology varies throughout Earth's lithosphere, and how this variation influences fault and shear zone behavior (e.g., Huntington et al., 2017), may be approached using a multitude of focused studies of exhumed and active structures alike.

Geoscientists generally agree that constitutive laws vary gradually in space and time through transitional regions (e.g., the brittle-ductile transition), rather than the abrupt change typically depicted by strength-depth diagrams (e.g., Scholz, 1988). Quantifying and characterizing these changes, however, has proven challenging. One possible approach would be to consider a series of outcrop exposures along a major fault system that was differentially exhumed, such as the Salzach-Ennstal-Mariazell-Puchberg fault system in Austria (Cole et al.,

418

419

420

421

422

423

424

425

426

427

428

429

430

431

432

433

434

435

436

437

438

439

440

| 2007; Frost et al., 2011). Alternatively, one could identify a series of isolated outcrop-scale |
|---|
| structures in a common lithology (e.g., granite), each exhumed from a different depth near and |
| within the brittle-ductile transition. In either case, the naturally deformed structures and |
| microstructures could inform a mechanical model to deduce representative constitutive laws and |
| conditions, similar to the example discussed in Section 2. |

Constitutive laws also are poorly constrained near Earth's surface, particularly within unconsolidated materials, such as soil or alluvium. Within this region, structural geologists have paid particular attention to secondary, echelon fractures that commonly form above ruptured strike-slip faults, referred to as "Riedel Shears" (e.g., Lin and Chiba, 2017). The criterion used to explain and interpret these features is Mohr-Coulomb failure (Tchalenko, 1970; Price and Cosgrove, 1990), which requires the fractures to form in shear. However, these fractures commonly preserve both opening and shear components, and may be related to tensile stresses near the fault tip (Martel and Boger, 1998). Thus, the origin and relevant constitutive laws for this deformation remain ambiguous. Though clay box experiments have reproduced Riedel fractures (e.g., Tchalenko, 1970), they are limited to length scales far smaller than what is observed in nature, which is problematic for both fracture scaling and pressure-dependent plastic yielding (e.g., Mohr-Coulomb). Another topic that recently piqued the interest of structural geologists is the physics controlling "off-fault deformation," the proportion of shear deformation accommodated by distributed mechanisms rather than discrete fault slip (e.g., Oskin et al., 2012). We propose that both of these topics could be addressed through mechanical models constrained by field measurements of recently activated faults.

Under all lithospheric conditions, it remains unclear how the constitutive properties of faults and shear zones evolve through time (e.g., Dolan and Haravitch, 2014; Erickson et al.,

| 2017). For example, do fault zones become weaker or stronger as they mature? One could adopt |
|---|
| a space-for-time approach to addressing this problem. In a uniform lithology, evaluating the |
| relative strength of fault zones with varying amounts of cumulative slip would reveal whether |
| more mature faults are stronger or weaker. This analysis would be enhanced by a combination of |
| laboratory experiments, microstructural analysis, and mechanical models compared to field data. |

Each of these research avenues will benefit from ongoing progress in mapping and computational capabilities. For example, recent advances in high-resolution imaging techniques – such as structure-from-motion photogrammetry (James and Robson, 2012; Westoby et al., 2012), optical image correlation (Leprince et al., 2007), and mobile laser scanning (Brooks et al., 2013) – allow for rapid, detailed mapping of structures across wide regions (e.g., Johnson et al., 2014; Milliner et al., 2015; Brooks et al., 2017). Increased computational power permits models with complex, non-linear constitutive laws that previously were impractical. In addition, continuum mechanical modeling packages – including open-source options (e.g., PyLith; https://geodynamics.org/cig/software/pylith) – are increasingly available, with improved documentation, support, and tutorials that ease the learning curve for new and experienced users.

5. Conclusions

While the disciplines of structural geology and continuum mechanics both were founded in the 18th century, the two fields saw little interaction over the next ~200 years. As a result, numerous outstanding questions remain in structural geology related to the mechanics of rock deformation. Crucial to mechanical analyses is the choice of constitutive law: the relationship between stress and strain, or stress and rate of deformation. Laboratory investigations have made great strides toward determining appropriate constitutive laws for geologic materials. By

| 463 | necessity, however, they are limited spatially, temporally, compositionally, and |
|-------------------|--|
| 464 | thermodynamically compared to conditions found in nature. Here, we have advocated for the use |
| 465 | of continuum mechanical models, informed by field measurements and microstructural analysis, |
| 466 | to evaluate representative constitutive laws under conditions ranging from Earth's surface to the |
| 467 | upper mantle. Future research will benefit from continuing technological advances in our |
| 468 | capacity to both map geologic structures and model complex geologic processes encountered |
| 469 | throughout the lithosphere. |
| 470 | Acknowledgements |
| 471 | We gratefully acknowledge Fred Pollitz, Brooks Proctor, and two anonymous reviewers |
| 472 | for their valuable feedback on this manuscript. Jessica Warren and Kathryn Kumamoto were |
| 473 | supported by the National Science Foundation under grants EAR-1255620 and EAR-1619880. |
| 474 | The field work complied with applicable legal requirements of the U. S. Government, and |
| 475 | relevant regulations for outcrop conservation from "A Code of Conduct for Rock Coring" by the |
| 476 | Geologists' Association. |
| 477 | References |
| 478 479 | Amadei, B., Stephansson, O., 1997. Rock Stress and its Measurement. Chapman & Hall, London. |
| 480 481 482 | Bell, D.R., Rossman, G.R., Maldener, J., Endisch, D., Rauch, F., 2003. Hydroxide in olivine: a quantitative determination of the absolute amount and calibration of the IR spectrum. Journal of Geophysical Research: Solid Earth 108. |
| 483 484 485 | Bemis, S.P., Micklethwaite, S., Turner, D., James, M.R., Akciz, S., Thiele, S.T., Bangash, H.A., 2014. Ground-based and UAV-based photogrammetry: A multi-scale, high-resolution mapping tool for structural geology and paleoseismology. J Struct Geol 69, 163-178. |
| 486 487 | Boettcher, M.S., Hirth, G., Evans, B., 2007. Olivine friction at the base of oceanic seismogenic zones. Journal of Geophysical Research: Solid Earth 112. |
| 488 489 | Brace, W.F., Kohlstedt, D.L., 1980. Limits on lithospheric stress imposed by laboratory experiments. Journal of Geophysical Research 85, 6248-6252. |

- Brooks, B.A., Glennie, C.L., Hudnut, K.W., Ericksen, T., Hauser, D., 2013. Mobile Laser
 Scanning Applied to the Earth Sciences. Eos 94, 313-315.
- Brooks, B.A., Minson, S.E., Glennie, C.L., Nevitt, J.M., Dawson, T., Rubin, R., Ericksen, T.L.,
 Lockner, D., Hudnut, K., Langenheim, V., 2017. Buried shallow fault slip from the South
 Napa earthquake revealed by near-field geodesy. Science Advances 3, e1700525.
- Brown, M., Smith, R., Aitken, A., 2002. Stratigraphical framework for the Devonian (Old Red
 Sandstone) rocks of Scotland south of a line from Fort William to Aberdeen, British
 Geological Survey Research Report, Keyworth, Nottingham, UK, p. 67.
- Bürgmann, R., Pollard, D.D., 1992. Influence of the state of stress on the brittle-ductile transition
 in granitic rock: Evidence from fault steps in the Sierra Nevada, California. Geology 20, 645 648.
- Bürgmann, R., Pollard, D.D., 1994. Strain accommodation about strike-slip fault discontinuities
 in granitic rock under brittle-ductile conditions. J Struct Geol 16, 1655-&.
- Bystricky, M., Lawlis, J., Mackwell, S., Heidelbach, F., Raterron, P., 2016. High temperature
 deformation of enstatite aggregates. Journal of Geophysical Research: Solid Earth 121, 6384 6400.
- Cole, J., Hacker, B., Ratschbacher, L., Dolan, J., Seward, G., Frost, E., Frank, W., 2007.
 Localized ductile shear below the seismogenic zone: Structural analysis of an exhumed
 strike-slip fault, Austrian Alps. J Geophys Res-Sol Ea 112.
- Coulomb, C.A., 1773. Sur une application des régles de maximis et minimis à quelques
 problémes de statique relatifs à l'architecture. Acad. Roy. des Sciences, Mémoires de math.
 et de physique par divers savants 7, 343-382.
- Cross, A., Skemer, P., 2017. Ultramylonite generation via phase mixing in high strain
 experiments. Journal of Geophysical Research: Solid Earth 122, 1744-1759.
- Cross, A.J., Kidder, S., Prior, D.J., 2015. Using microstructures and TitaniQ thermobarometry of
 quartz sheared around garnet porphyroclasts to evaluate microstructural evolution and
 constrain an Alpine Fault Zone geotherm. J Struct Geol 75, 17-31.
- Cyprych, D., Piazolo, S., Wilson, C.J., Luzin, V., Prior, D.J., 2016. Rheology, microstructure and
 crystallographic preferred orientation of matrix containing a dispersed second phase: Insight
 from experimentally deformed ice. Earth Planet Sc Lett 449, 272-281.
- Dawers, N.H., Anders, M.H., Scholz, C.H., 1993. Growth of normal faults: Displacement-length
 scaling. Geology 21, 1107-1110.
- Dolan, J.F., Haravitch, B.D., 2014. How well do surface slip measurements track slip at depth in large strike-slip earthquakes? The importance of fault structural maturity in controlling onfault slip versus off-fault surface deformation. Earth Planet Sc Lett 388, 38-47.
- Drucker, D.C., Prager, W., 1952. Soil mechanics and plastic analysis or limit design. Quarterly
 of Applied Mathematics 10, 157-165.
- Erickson, B.A., Dunham, E.M., Khosravifar, A., 2017. A finite difference method for off-fault
 plasticity throughout the earthquake cycle. Journal of the Mechanics and Physics of Solids
 109, 50-77.
- Frost, E., Dolan, J., Ratschbacher, L., Hacker, B., Seward, G., 2011. Direct observation of fault
 zone structure at the brittle-ductile transition along the Salzach-Ennstal-Mariazell-Puchberg
 fault system, Austrian Alps. J Geophys Res-Sol Ea 116.
- Griffith, W.A., Di Toro, G., Pennacchioni, G., Pollard, D.D., 2008. Thin pseudotachylytes in
 faults of the Mt. Abbot quadrangle, Sierra Nevada: Physical constraints for small seismic slip
 events. J Struct Geol 30, 1086-1094.

- 536 Griggs, D., 1939. Creep of rocks. The Journal of Geology 47, 225-251.
- Grigull, S., Ellis, S.M., Little, T.A., Hill, M.P., Buiter, S.J.H., 2012. Rheological constraints on
 quartz derived from scaling relationships and numerical models of sheared brittle-ductil
- 539 quartz veins, central Southern Alps, New Zealand. J Struct Geol 37, 200-222.
- Hansen, L., Zimmerman, M., Kohlstedt, D.L., 2011. Grain boundary sliding in San Carlos
 olivine: Flow law parameters and crystallographic preferred orientation. Journal of
 Geophysical Research: Solid Earth 116.
- Hansen, L.N., Warren, J.M., 2015. Quantifying the effect of pyroxene on deformation of
 peridotite in a natural shear zone. Journal of Geophysical Research: Solid Earth 120, 2717 2738.
- Hansen, L.N., Zhao, Y.-H., Zimmerman, M.E., Kohlstedt, D.L., 2014. Protracted fabric
 evolution in olivine: Implications for the relationship among strain, crystallographic fabric,
 and seismic anisotropy. Earth and Planetary Science Letters 387, 157-168.
- Hirth, G., Kohlstedt, D., 2003. Rheology of the upper mantle and the mantle wedge: A view
 from the experimentalists. Inside the subduction Factory, 83-105.
- Hirth, G., Teyssier, C., Dunlap, W.J., 2001. An evaluation of quartzite flow laws based on
 comparisons between experimentally and naturally deformed rocks. International Journal of
 Earth Sciences 90, 77-87.
- Hobbs, B.E., Ord, A., 2014. Structural geology: the mechanics of deforming metamorphic rocks.
 Elsevier.
- 556 Hubbert, M.K., 1972. Structural Geology. Hafner Publishing Company, New York.
- Hughes, T.J.R., 2000. The Finite Element Method: Linear Static and Dynamic Finite Element
 Analysis. Dover Publications, Inc., Mineola, NY.
- Huntington, K.W., Klepeis, K.A., contributors, c., 2017. Challenges and opportunities for
 research in tectonics: Understanding deformation and the processes that link Earth systems,
 from geologic time to human time. A community vision document submitted to the U.S.
 National Science Foundation.
- Jaeger, J.C., Cook, N.G., Zimmerman, R., 2009. Fundamentals of rock mechanics, 4th ed. John
 Wiley & Sons.
- James, M., Robson, S., 2012. Straightforward reconstruction of 3D surfaces and topography with
 a camera: Accuracy and geoscience application. Journal of Geophysical Research: Earth
 Surface 117.
- Ji, S., Xia, B., 2002. Rheology of Polyphase Earth Materials. Polytechnic International Press,
 Montreal, Canada.
- Johnson, A.M., 1970. Physical Processes in Geology. Freeman, Cooper & Company, San
 Francisco, CA.
- Johnson, K., Nissen, E., Saripalli, S., Arrowsmith, J.R., McGarey, P., Scharer, K., Williams, P.,
 Blisniuk, K., 2014. Rapid mapping of ultrafine fault zone topography with structure from
 motion. Geosphere 10, 969-986.
- Karato, S.i., Toriumi, M., Fujii, T., 1980. Dynamic recrystallization of olivine single crystals
 during high temperature creep. Geophys Res Lett 7, 649-652.
- Kelemen, P.B., Dick, H.J., 1995. Focused melt flow and localized deformation in the upper
 mantle: Juxtaposition of replacive dunite and ductile shear zones in the Josephine peridotite,
- 579 SW Oregon. Journal of Geophysical Research: Solid Earth 100, 423-438.

- Kenis, I., Urai, J.L., van der Zee, W., Hilgers, C., Sintubin, M., 2005. Rheology of fine-grained
 siliciclastic rocks in the middle crust—evidence from structural and numerical analysis. Earth
 Planet Sc Lett 233, 351-360.
- 583 Kirby, S.H., 1983. Rheology of the lithosphere. Reviews of Geophysics 21, 1458-1487.
- Kohlstedt, D., Goetze, C., 1974. Low stress high temperature creep in olivine single crystals.
 Journal of Geophysical Research 79, 2045-2051.
- Kohlstedt, D.L., Evans, B., Mackwell, S.J., 1995. Strength of the lithosphere: Constraints
 imposed by laboratory experiments. J Geophys Res-Sol Ea 100, 17587-17602.
- 588 Kumamoto, K., 2018. Exploring the rheological properties of the upper mantle: From the field to 589 the laboratory. Stanford University.
- Lai, W.M., Rubin, D.H., Krempl, E., 2009. Introduction to continuum mechanics. Butterworth Heinemann.
- Leprince, S., Ayoub, F., Klinger, Y., Avouac, J.-P., 2007. Co-registration of optically sensed
 images and correlation (COSI-Corr): An operational methodology for ground deformation
 measurements, Geoscience and Remote Sensing Symposium, 2007. IGARSS 2007. IEEE
 International. IEEE, pp. 1943-1946.
- Lin, A., Chiba, T., 2017. Coseismic conjugate faulting structures produced by the 2016 M w 7.1
 Kumamoto earthquake, Japan. J Struct Geol 99, 20-30.
- 598 Linckens, J., Bruijn, R.H., Skemer, P., 2014. Dynamic recrystallization and phase mixing in 599 experimentally deformed peridotite. Earth Planet Sc Lett 388, 134-142.
- 600 Lister, G.S., Snoke, A.W., 1984. S-C mylonites. J Struct Geol 6, 617-638.
- Lockwood, J.P., Lydon, P.A., 1975. Geologic map of the Mount Abbot Quadrangle, central
 Sierra Nevada, California, United States Geological Survey Quadrangle Map GQ-1155.
- Loney, R.A., Himmelberg, G.R., 1976. Structure of the Vulcan Peak alpine-type peridotite,
 southwestern Oregon. Geol Soc Am Bull 87, 259-274.
- Malvern, L.E., 1969. Introduction to the Mechanics of a Continuous Medium. Prentice-Hall,
 Inc., Englewood Cliffs, New Jersey.
- Mancktelow, N.S., Pennacchioni, G., 2010. Why calcite can be stronger than quartz. Journal of
 Geophysical Research: Solid Earth 115.
- Martel, S.J., Boger, W.A., 1998. Geometry and mechanics of secondary fracturing around small
 three-dimensional faults in granitic rock. J Geophys Res-Sol Ea 103, 21299-21314.
- McIntyre, D., McKirdy, A., 2012. James Hutton—The founder of modern geology. National
 Museums Scotland Enterprises Limited, Edinburgh.
- 613 Milliner, C.W.D., Dolan, J.F., Hollingsworth, J., Leprince, S., Ayoub, F., Sammis, C.G., 2015.
- Quantifying near-field and off-fault deformation patterns of the 1992 M-w 7.3 Landers earthquake. Geochem Geophy Geosy 16, 1577-1598.
- Nevitt, J.M., Pollard, D.D., 2017. Impacts of off-fault plasticity on fault slip and interaction at the base of the seismogenic zone. Geophys Res Lett 44, 1714-1723.
- Nevitt, J.M., Pollard, D.D., Warren, J.M., 2014. Evaluation of transtension and transpression within contractional fault steps: Comparing kinematic and mechanical models to field data. J Struct Geol 60, 55-69.
- 621 Nevitt, J.M., Warren, J.M., Kidder, S., Pollard, D.D., 2017a. Comparison of thermal modeling,
- 622 microstructural analysis, and Ti-in-quartz thermobarometry to constrain the thermal history
- of a cooling pluton during deformation in the Mount Abbot Quadrangle, CA. Geochem
- 624 Geophy Geosy 18, 1270-1297.

- Nevitt, J.M., Warren, J.M., Pollard, D.D., 2017b. Testing constitutive equations for brittle ductile deformation associated with faulting in granitic rock. Journal of Geophysical Research: Solid Earth.
- Newton, I., 1999. The Principia, mathematical principles of natural philosophy, a new translation. University of California, Berkeley, CA.
- Ohuchi, T., Kawazoe, T., Higo, Y., Funakoshi, K.-i., Suzuki, A., Kikegawa, T., Irifune, T., 2015.
 Dislocation-accommodated grain boundary sliding as the major deformation mechanism of olivine in the Earth's upper mantle. Science advances 1, e1500360.
- Oskin, M.E., Arrowsmith, J.R., Corona, A.H., Elliott, A.J., Fletcher, J.M., Fielding, E.J., Gold,
 P.O., Garcia, J.J.G., Hudnut, K.W., Liu-Zeng, J., 2012. Near-field deformation from the El
 Mayor-Cucapah earthquake revealed by differential LIDAR. Science 335, 702-705.
- Passchier, C.W., Trouw, R.A.J., 2006. Microtectonics, 2 ed. Springer-Verlag, Berlin, Heidelberg,
 New York.
- Paterson, M., 1958. Experimental deformation and faulting in Wombeyan marble. Geol Soc Am Bull 69, 465-476.
- Paterson, M.S., 1987. Problems in the Extrapolation of Laboratory Rheological Data.
 Tectonophysics 133, 33-43.
- Paterson, M.S., Wong, T.-f., 2005. Experimental rock deformation-the brittle field. Springer Verlag, Berlin.
- Pennacchioni, G., Zucchi, E., 2013. High temperature fracturing and ductile deformation during
 cooling of a pluton: The Lake Edison granodiorite (Sierra Nevada batholith, California). J
 Struct Geol 50, 54-81.
- Pollard, D.D., Fletcher, R.C., 2005. Fundamentals of structural geology. Cambridge University
 Press, Cambridge, UK.
- 649 Price, N.J., Cosgrove, J.W., 1990. Analysis of geological structures. Cambridge University Press.
- Raleigh, C., Kirby, S., Carter, N., Lallemant, H., 1971. Slip and the clinoenstatite transformation
 as competing rate processes in enstatite. Journal of Geophysical Research 76, 4011-4022.
- 652 Ramsay, J., 1980. Shear zone geometry: a review. J Struct Geol 2, 83-99.
- Ramsay, J.G., Lisle, R., 2000. The techniques of modern structural geology. Volume 3:
 Applications of continuum mechanics in structural geology. Academic, San Diego, Calif.
- Recanati, A., Kurz, M., Warren, J., Curtice, J., 2012. Helium distribution in a mantle shear zone from the Josephine Peridotite. Earth Planet Sc Lett 359, 162-172.
- Rowe, C.D., Meneghini, F., Moore, J.C., 2011. Textural record of the seismic cycle: Strain-rate
 variation in an ancient subduction thrust. Geological Society, London, Special Publications
 359, 77-95.
- Scholz, C., 1988. The brittle-plastic transition and the depth of seismic faulting. Geologische
 Rundschau 77, 319-328.
- Segall, P., Pollard, D.D., 1980. Mechanics of discontinuous faults. Journal of Geophysical
 Research 85, 4337-4350.
- Segall, P., Pollard, D.D., 1983. Nucleation and growth of strike slip faults in granite. Journal of
 Geophysical Research 88, 555-568.
- Sibson, R.H., 1982. Fault Zone Models, Heat-Flow, and the Depth Distribution of Earthquakes in
 the Continental-Crust of the United-States. Bulletin of the Seismological Society of America
 72, 151-163.
- 669 Sibson, R.H., 1983. Continental Fault Structure and the Shallow Earthquake Source. Journal of 670 the Geological Society 140, 741-767.

- Skemer, P., Karato, S.-i., 2007. Effects of solute segregation on the grain-growth kinetics of
 orthopyroxene with implications for the deformation of the upper mantle. Physics of the
 Earth and Planetary Interiors 164, 186-196.
- Skemer, P., Warren, J.M., Hansen, L.N., Hirth, G., Kelemen, P.B., 2013. The influence of water
 and LPO on the initiation and evolution of mantle shear zones. Earth Planet Sc Lett 375, 222 233.
- 677 Skemer, P., Warren, J.M., Kelemen, P.B., Hirth, G., 2010. Microstructural and rheological 678 evolution of a mantle shear zone. Journal of Petrology 51, 43-53.
- Tchalenko, J., 1970. Similarities between shear zones of different magnitudes. Geol Soc Am Bull
 81, 1625-1640.
- Tikoff, B., Larson, C.E., Newman, J., Little, T., 2010. Field-based constraints on finite strain and
 rheology of the lithospheric mantle, Twin Sisters, Washington. Lithosphere 2, 418-422.
- Toriumi, M., 1979. Relation between dislocation density and subgrain size of naturally deformed olivine in peridotites. Contributions to mineralogy and petrology 68, 181-186.
- Treagus, S.H., 1999. Are viscosity ratios of rocks measurable from cleavage refraction? J Struct
 Geol 21, 895-901.
- Tullis, J., 2002. Deformation of granitic rocks: experimental studies and natural examples, in:
 Karato, S.-i., Wenk, H.-R. (Eds.), Plastic Deformation of Minerals and Rocks. Mineralogical
 Society of America, pp. 51–96.
- Tullis, T.E., Tullis, J., 1986. Experimental rock deformation techniques. Mineral and Rock
 Deformation: Laboratory Studies: The Paterson Volume, 297-324.
- 692 Turcotte, D., Schubert, G., 2014. Geodynamics. Cambridge University Press.
- Van der Wal, D., Chopra, P., Drury, M., Gerald, J.F., 1993. Relationships between dynamically
 recrystallized grain size and deformation conditions in experimentally deformed olivine
 Geophys Res Lett 20, 1479-1482.
- Von Mises, R., 1913. Mechanik der festen Körper im plastisch deformablen Zustand. Göttin.
 Nachr. Math. Phys. Kl. 1913, 582-592.
- Wallis, D., Hansen, L.N., Britton, T.B., Wilkinson, A.J., 2017. Dislocation Interactions in
 Olivine Revealed by HR EBSD. Journal of Geophysical Research: Solid Earth.
- Warren, J.M., Hauri, E.H., 2014. Pyroxenes as tracers of mantle water variations. Journal of
 Geophysical Research: Solid Earth 119, 1851-1881.
- Warren, J.M., Hirth, G., 2006. Grain size sensitive deformation mechanisms in naturally
 deformed peridotites. Earth Planet Sc Lett 248, 438-450.
- Warren, J.M., Hirth, G., Kelemen, P.B., 2008. Evolution of olivine lattice preferred orientation
 during simple shear in the mantle. Earth Planet Sc Lett 272, 501-512.
- Westoby, M., Brasington, J., Glasser, N., Hambrey, M., Reynolds, J., 2012. 'Structure-from Motion' photogrammetry: A low-cost, effective tool for geoscience applications.
 Geomorphology 179, 300-314.
- Zhao, N., Hirth, G., Cooper, R., Kruckenberg, S., 2017. Grain Boundary Sliding in Olivine+
 Clinopyroxene Aggregates: Weakening Mechanism and Microstructure, AGU Fall Meeting
 Abstracts.

Figures and Captions



 Figure 1. Hutton's unconformity at Siccar Point, Scotland. Vertical Silurian strata are overlain by a basal conglomerate and the gently inclined Devonian strata. Dashed yellow line marks angular unconformity, a 65 Ma hiatus in time. Photograph ©Lorne Gill/SNH.



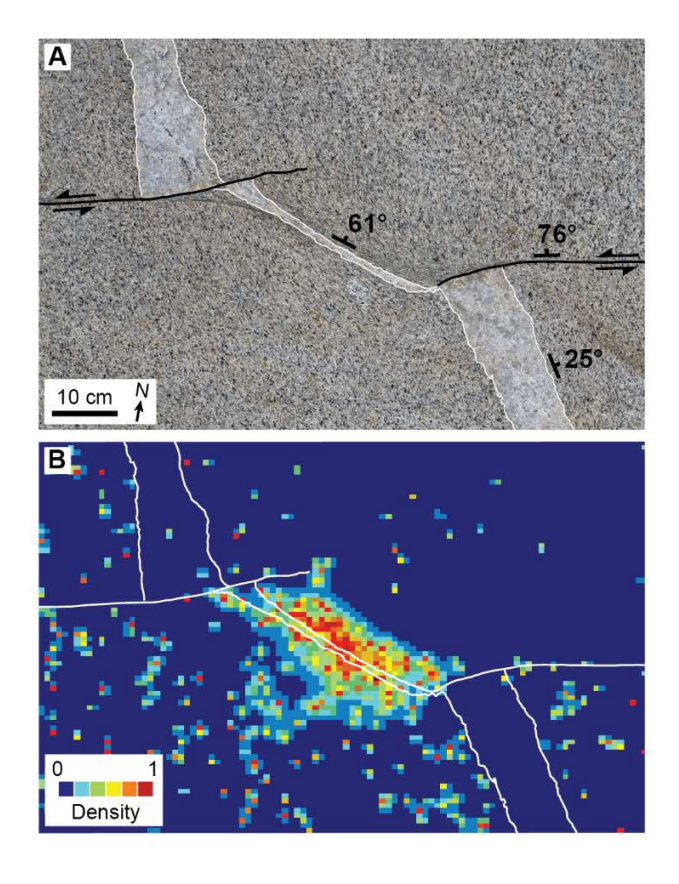


Figure 2. Seven Gables outcrop (37°19 27.08 N 118°50 39.52 W). (A) Orthorectified photo with faults and dike outlined in black and white, respectively. (B) Normalized density distribution of fault-related fabric, defined by mafic grains with aspect ratios >3 and orientations between 260-305°, as determined using the MATLAB image analysis toolbox. Modified from Nevitt et al. (2017b).



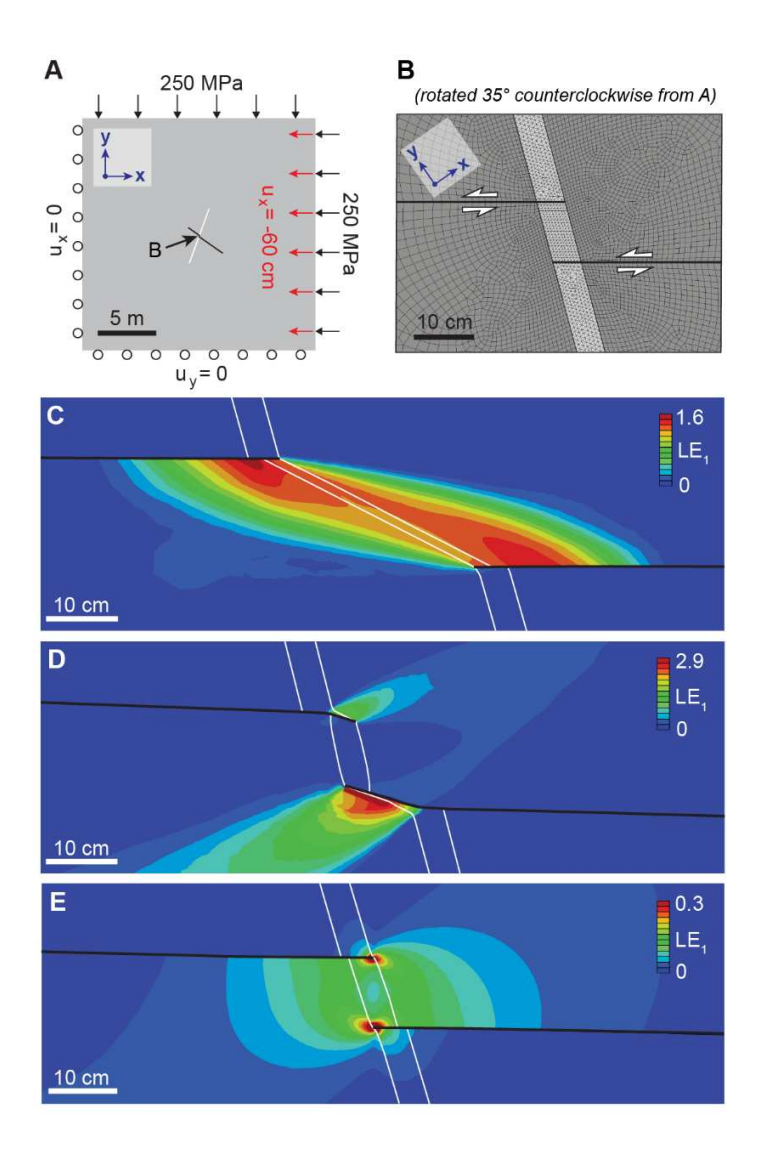


Figure 3. Finite element model set-up and results. (A) Dimensions, geometry, and boundary conditions employed in each model. Dike and faults are represented by white and black lines, respectively. First, the model equilibrates to a lithostatic pressure of 250 MPa. Then, the model is contracted at a 35° angle to the faults to instigate fault slip. This is done by displacing the right model boundary by 60 cm in the negative-x direction (indicated by red arrows). (B) Detailed view of the geometry and mesh in the center of model domain. Note that the model is rotated 35° counterclockwise relative to (A) for a view analogous to Figure 2. (C-E) Maximum logarithmic strain for (C) Von Mises elastoplasticity, (D) Drucker-Prager elastoplasticity, and (E) Power-law creep viscoelasticity. Please refer to Nevitt et al. (2017b) for parameters used.

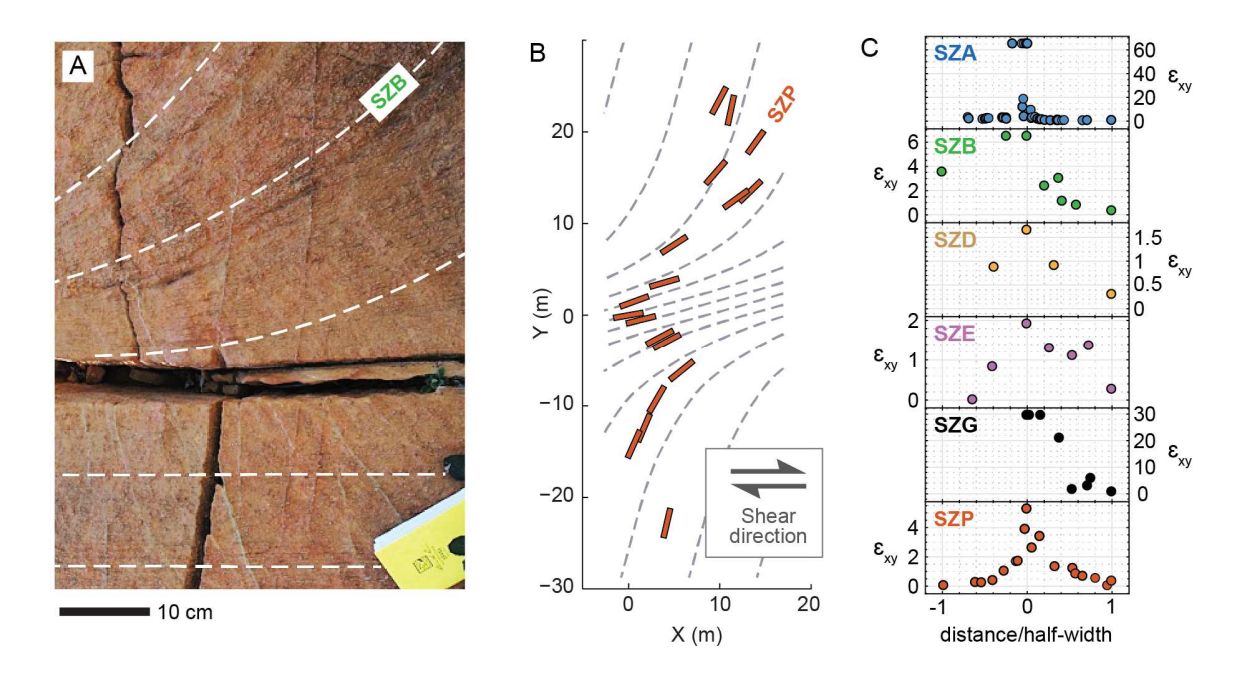


Figure 4. (A) Outcrop photo of shear zone B (max strain of 6.5) in the Josephine Peridotite.

Dashed white lines indicate the deflection of pyroxene foliation. (B) Structural cross-section of

shear zone P, perpendicular to the shear plane. Orange lines indicate the measured strike of pyroxene foliation. Grey dashed lines represent the schematic deflection of foliation across the

shear zone. (C) Strain profiles as a function of distance for 6 shear zones, based on field

measurements of pyroxene foliation projected onto the X-Y structural section perpendicular to the shear plane. Half-width is calculated as the distance in the positive direction from the

location of maximum shear strain at which shear strain decreases below 0.2. In SZA and SZG,

strain is capped at 65 and 30, respectively, due to sub-vertical foliation measurements. Data are

from Warren et al. (2008), Skemer et al. (2010), Recanati et al. (2012), and our new data

(Supporting Material).

739

740

741

742

743744

745

746747

748749750

751752

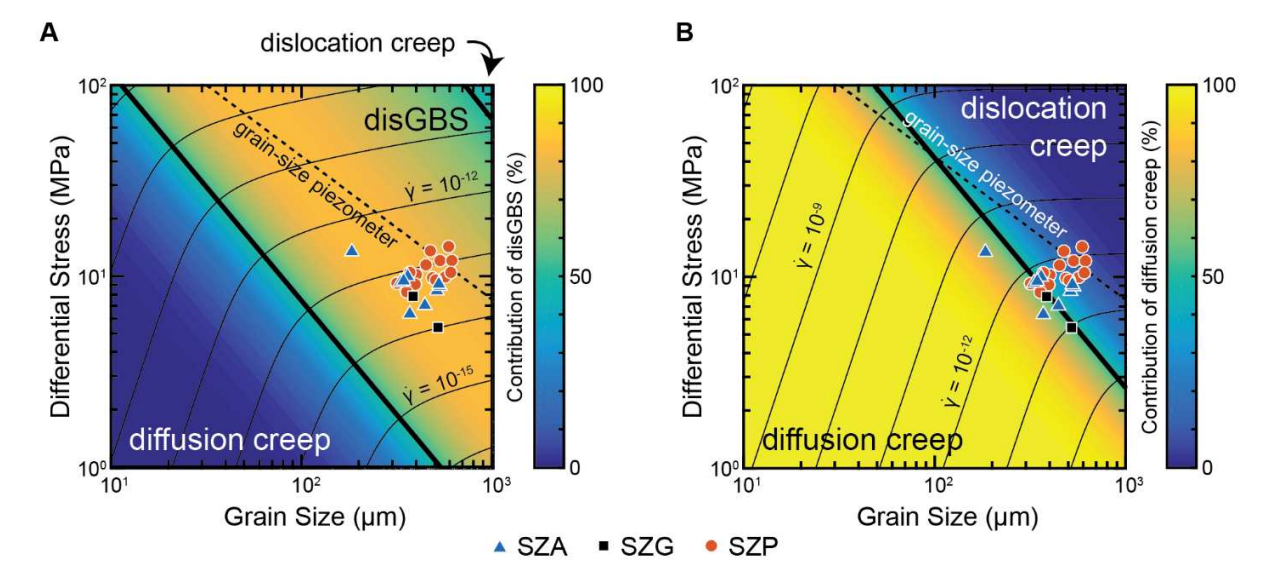


Figure 5. Comparison of microstructural data from three shear zones (SZA, SZG, and SZP; strain profiles are shown in Figure 4) to laboratory-derived olivine flow laws. Deformation mechanism maps are for (A) anhydrous and (B) hydrous (400 ppm H/Si or 25 ppm H₂O) conditions at 1000°C and 1 GPa (30 km depth). Shading indicates the relative contribution of grain size-sensitive deformation mechanisms: disGBS in (A) and diffusion creep in (B). Flow laws are from Hirth and Kohlstedt (2003) and Hansen et al. (2011), with the wet flow laws adjusted for the revised water calibration of Bell et al. (2003). Stress for the Josephine Peridotite samples is calculated using the subgrain size piezometer of Toriumi (1979), with the grain size piezometer (Karato et al., 1980; Van der Wal et al., 1993) shown for comparison. Data for Josephine samples are from Skemer et al. (2010), Hansen and Warren (2015), and Kumamoto (2018).



| 1 | Nevitt, J.M., J.M. Warren, K.M. Kumamoto, and D.D. Pollard, "Using geologic structures to |
|---|---|
| 2 | constrain constitutive laws not accessible in the laboratory," for submission to Journal of |
| 3 | Structural Geology. |
| 4 | |
| 5 | Highlights |
| 6 | Natural structures provide bases for mechanical models to test constitutive laws |
| 7 | Methodology is applicable in all lithologies throughout the lithosphere |
| 8 | Granodiorite exhumed from mid-crust shows plastic yielding enhances fault slip |
| 9 | Deformation observed in exhumed mantle conflicts with empirical constitutive laws |

• Technological advances will propel this methodology throughout the 21st century